Chinese Chemical Letters 33 (2022) 2747–2752

Contents lists available at ScienceDirect

Chinese Chemical Letters

journal homepage: www.elsevier.com/locate/cclet

Ordered mesoporous carbon as an efficient heterogeneous catalyst to activate peroxydisulfate for degradation of sulfadiazine

Zhi-Ling Li[a], Di Cao[a], Hao Cheng[a], Fan Chen[a,c], Jun Nan[a], Bin Liang[b], Kai Sun[d,*], Cong Huang[e], Ai-Jie Wang[a,b,*]

[a] State Key Laboratory of Urban Water Resource and Environment, School of Environment, Harbin Institute of Technology, Harbin 150090, China
[b] School of Civil & Environmental Engineering, Harbin Institute of Technology (Shenzhen), Shenzhen 518055, China
[c] School of Ecology and Environment, Northwestern Polytechnical University, Xi'an 710129, China
[d] Key Lab of Structures Dynamic Behavior and Control of China Ministry of Education, School of Civil Engineering, Harbin Institute of Technology, Harbin 150090, China
[e] National Technology Innovation Center of Synthetic Biology, Tianjin Institute of Industrial Biotechnology, Chinese Academy of Sciences, Tianjin 300308, China

ARTICLE INFO

Article history:
Received 21 August 2021
Revised 25 September 2021
Accepted 27 October 2021
Available online 2 November 2021

Keywords:
Ordered mesoporous carbon CMK
Sulfadiazine
Peroxydisulfate
Degradation pathway
Density functional theory
Physicochemical properties

ABSTRACT

Catalytic potential of carbon nanomaterials in peroxydisulfate (PDS) advanced oxidation systems for degradation of antibiotics remains poorly understood. This study revealed ordered mesoporous carbon (type CMK) acted as a superior catalyst for heterogeneous degradation of sulfadiazine (SDZ) in PDS system, with a first-order reaction kinetic constant (k) and total organic carbon (TOC) mineralization efficiency of 0.06 min^{-1} and 59.67% ± 3.4% within 60 min, respectively. CMK catalyzed PDS system exhibited high degradation efficiencies of five other sulfonamides and three other types of antibiotics, verifying the broad-degradation capacity of antibiotics. Under neutral pH conditions, the optimal catalytic parameters were an initial SDZ concentration of 44.0 mg/L, CMK dosage of 0.07 g/L, and PDS dosage of 5.44 mmol/L, respectively. X-ray photoelectron spectroscopy and Raman spectrum analysis confirmed that the defect structure at edge of CMK and oxygen-containing functional groups on surface of CMK were major active sites, contributing to the high catalytic activity. Free radical quenching analysis revealed that both $SO_4^{\bullet-}$ and $^{\bullet}OH$ were generated and participated in catalytic reaction. In addition, direct electron transfer by CMK to activate PDS also occurred, further promoting catalytic performance. Configuration of SDZ molecule was optimized using density functional theory, and the possible reaction sites in SDZ molecule were calculated using Fukui function. Combining ultra-high-performance liquid chromatography (UPLC)–mass spectrometry (MS)/MS analysis, three potential degradation pathways were proposed, including the direct removal of SO_2 molecules, the 14S-17 N fracture, and the 19C-20 N and 19C-27 N cleavage of the SDZ molecule. The study demonstrated that ordered mesoporous carbon could work as a feasible catalytic material for PDS advanced oxidation during removal of antibiotics from wastewater.

Sulfonamides are one of the most commonly used antibiotic groups in aquaculture [1], animal husbandry, and human medicine [2]. Most sulfonamides are polar amphoteric compounds that are chemically stable, resistant to biodegradation, and carcinogenic [3,4], thus posing a serious threat to humans and ecosystems [5]. Sulfadiazine (SDZ) is one of the typical sulfonamide that has been extensively applied worldwide [6]. As a result of incomplete utilization, numerous SDZ entered environment each year. Presence of SDZ in ambient environment could be harmful to resident aquatic organisms and humans, and may even induce antibiotic-resistant genes. SDZ was detected at ng/L-μg/L levels in secondary effluent of sewage treatment plants [7]. In antibiotic-heavily contaminated areas, like pharmaceutical wastewater, concentration of antibiotics is reported that approach as high as hundreds mg/L [8].

The occurrence of antibiotics with bio-toxic characteristics in wastewater treatment plants (WWTPs) inevitably causes a low biological treatment efficiency and can even lead to the collapse of the bio-treatment system [9]. Therefore, pretreatment or control is necessary to reduce or remove the residual risk and avoid further pollution of surface water [10]. The commonly applied technologies to treat sulfadiazine and other types of antibiotics-contaminated wastewater including biological process, adsorption,

* Corresponding authors.
E-mail addresses: sunkai@hit.edu.cn (K. Sun), waj0578@hit.edu.cn (A.-J. Wang).

https://doi.org/10.1016/j.cclet.2021.10.086
1001-8417/

Photolysis, ozonization, chlorination and advanced oxidation processes (AOPs) [11], owing to their strong oxidation capacities (E_0 of 2.5–3.1 V) [12], high chemical stabilities, and high selectivity [13,14], advanced oxidation processes based on peroxydisulfate (PDS) have been developed to deal with refractory organic compounds. Metal-based materials and carbon-based materials are the most commonly used materials for catalyzing PDS [15–17]. Because metal-based materials possess low catalytic activities and may pose a pollution risk due to metal leaching [18], carbon-based materials that are environmentally friendly and possess high catalytic activities have been applied for the decomposition and transformation of various types of refractory pollutants [19,20]. Among them, biochars have been reported to effectively activate PDS for the degradation of antibiotics, such as SDZ, sulfamethoxazole (SMX), bisphenol A, and 4-chlorophenol [21,22]. However, the application of biochar should consider potential environmental risks, including the dissolution of carcinogenic and teratogenic substances, such as polycyclic aromatic hydrocarbons (PAHs) and heavy metals [23]. Recently, carbon nanomaterials have been developed as an alternative to catalyze PDS [24], including ordered mesoporous carbon (OMC, type CMK), fullerenes, single-walled carbon nanotubes (SWCNTs), multi-walled carbon nanotubes (MWCNTs), nanodiamonds (NDs), and so on [19,25,26]. Previous studies have reported the effectiveness of nitrobenzene- and phenol-containing petrochemical wastewaters using carbon nanomaterial-activated PDS 27–29]. Among them, OMC is popular because of its high pore volume and excellent free radical conduction capacity [30,31]. However, whether these carbon nanomaterials can activate PDS to facilitate or promote the heterogeneous degradation of sulfonamides or other types of antibiotics remains poorly understood. In addition, the optimal conditions and enhanced degradation-related catalytic mechanism are largely unknown.

Therefore, we constructed a PDS advanced oxidation system, and the catalytic activities of four carbon nanomaterials for degradation of SDZ. Besides SDZ, different kinds of sulfonamides, as well as three other antibiotics with different structures and bacteriostatic performance, namely, chlortetracycline hydrochloride (CTC), ciprofloxacin (CIP) and amoxicillin (AMX), as representatives of tetracyclines, fluoroquinolones and β-lactams, respectively, were selected as aim pollutants to investigate CMK/PDS degradation spectrum. The most favorable carbon nanomaterial was selected, and its catalytic performance, antibiotic treatment range, and optimal catalytic conditions were identified. The activation mechanism and degradation pathway were proposed *via* analysis of the free radical quenching properties, density functional theory, and ultra-high-performance liquid chromatography-tandem mass spectrometry (UPLC-MS/MS) analysis.

The main reagent, characterization of CMK, experimental procedure, and analysis methods are exhibited in the Supporting information. The performance of SDZ removal under each type of nanocarbon material (CMK, SWCNTs, NDs, and MWCNTs) as a catalyst of PDS is shown in Fig. S1A (Supporting information). The results showed that SDZ removal via adsorption on PDS was negligible within 120 min. In addition, SDZ was barely adsorbed by NDs or MWCNTs alone, which agreed with a previous study that found that NDs and MWCNTs showed poor performance for the adsorption of organic contaminants [28]. A low removal efficiency (17.3% ± 4.3%) of SDZ was observed in 120 min using the NDs/PDS system, suggesting that NDs could not activate PDS efficiently. A moderate removal efficiency (44.8% ± 4.0%) of SDZ was found using the MWCNTs/PDS system, which was consistent with previous results [32]. A removal efficiency of 53.7% ± 4.2% was determined for SWCNTs alone, whereas this was just 28.5% ± 4.1% for CMK alone. However, an apparent increase in SDZ removal (up to 97.0% ± 2.3% and 100%) was achieved when SWCNTs and CMK were used in the PDS system, suggesting that both could effectively activate persulfate to degrade SDZ. The CMK/PDS system exhibited the highest degradation efficiency and the smallest adsorption, contributing to the highest catalytic and oxidative performance. The plot data of SDZ removal in CMK/PDS systems were well fitted with the pseudo-first-order kinetics model ($R^2 = 0.993$) (Fig. S1B in Supporting information). The apparent rate constant (k) was calculated to be 0.06 min^{-1}, reflecting the high treatment efficiency. Such, CMK was selected as the optimal catalyst.

Fig. S2 (Supporting information) shows the degradation potential of the other commonly applied antibiotics in the CMK/PDS system, except for SDZ. The degradation efficiencies of the other five sulfonamides within 120 min were 94.5% ± 2.1% (SA), 89.8% ± 2.6% (SPD), 94.5% ± 3.0% (SMR), 95.5% ± 1.9% (SMT), and 90.8% ± 2.4% (SMX), indicating the feasible degradation capacity of the system for these sulfonamides. The degradation efficiencies of the other types of antibiotics with different chemical structures were also analyzed, as shown in Fig. S3 (Supporting information). Among them, ciprofloxacin was completely removed within 45 min, corresponding to the highest degradation efficiency. In comparison, 89.7% ± 2.7% of amoxicillin and 87.3% ± 2.4% of chlortetracycline hydrochloride were removed in 120 min, indicating the potential of the CMK/PDS system to degrade antibiotics with different structures.

Fig. 1A shows that the mineralization efficiency of the CMK/PDS system approached 65.7% ± 3.7% within 60 min, which was maintained until 120 min, verifying the generation of organic intermediates that were hardly further degraded. Fig. 1B displays the consumption of PDS in the systems with or without CMK or SDZ. When CMK was not added, only 0.4% ± 0.06% of PDS was consumed, implying that PDS alone could hardly degrade SDZ. In the absence of SDZ, a certain amount of PDS (7.0% ± 0.6%) was consumed, indicating that CMK could consume some of the PDS by forming highly reactive sulfate even without SDZ. The highest consumption of PDS (12.0% ± 0.56%) was observed in the presence of both CMK and SDZ, suggesting the accelerated consumption of PDS in the presence of SDZ. Fig. 1C shows that after three cycles of repeated use, a removal efficiency of 48.0% ± 3.1% for SDZ could be steadily maintained, implying the reuse potential of CMK. The decreased activity of CMK could be attributed to the decreased number of active sites due to surface chemical composition changes or the adsorption of generated intermediates [28].

As shown in Fig. 2A, the dosing concentrations of SDZ were 20 mg/L, 50 mg/L, 100 mg/L, 200 mg/L, respectively, to evaluate the catalytic performance of CMK. A degradation rate of 98.4% ± 2.0% at an SDZ concentration of 20 mg/L was obtained within 5 min. As the SDZ concentration increased to 200 mg/L, the removal efficiency decreased to 37.6% ± 4.4%, revealing a negative correlation between the removal efficiency and SDZ concentration. Previously, some studies found the high pollutant concentration would induce occupation of active sites of CMK, restricting its catalytic activity [33]. There was a positive correlation between SDZ removal efficiency and PDS concentration; as the PDS concentration increased, the SDZ removal efficiency increased, and almost complete degradation was obtained within 30 min (Fig. 2B). When the SDZ concentration was low, the capacity of the CMK/PDS system was not fully utilized. When the SDZ concentration was high, the processing efficiency may have been limited by the number of reaction sites and the free radical concentration. Similarly, the increased dosage of CMK improved the SDZ removal efficiency, and SDZ was completely degraded within just 5 min at a CMK dosage of 0.2 g/L (Fig. 2C). The enhanced performance may be attributable to an increased number of active sites supplied by the high dosage of CMK.

As shown in Fig. 2D, the highest removal efficiency of SDZ (88.8% ± 3.4% within 10 min) was obtained at pH 3.0, whereas an increased pH resulted in a decreased SDZ degradation rate. The removal efficiency of SDZ was 94.2% ± 3.0% within 45 min at pH

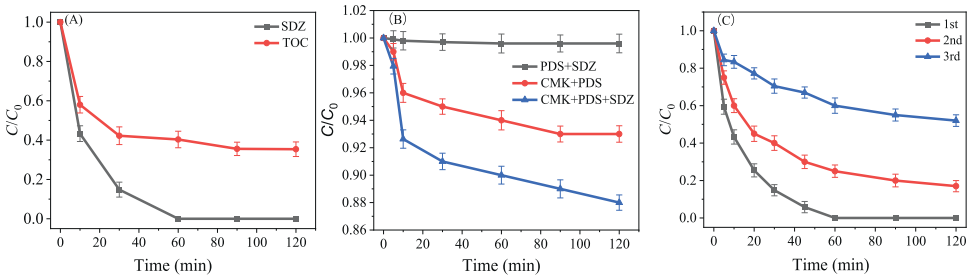

Fig. 1. (A) The degradation and mineralization degree of CMK/PDS system. (B) The consumption of PDS under systems with and without CMK or SDZ. (C) The degradation of SDZ by the repeated utilization of CMK.

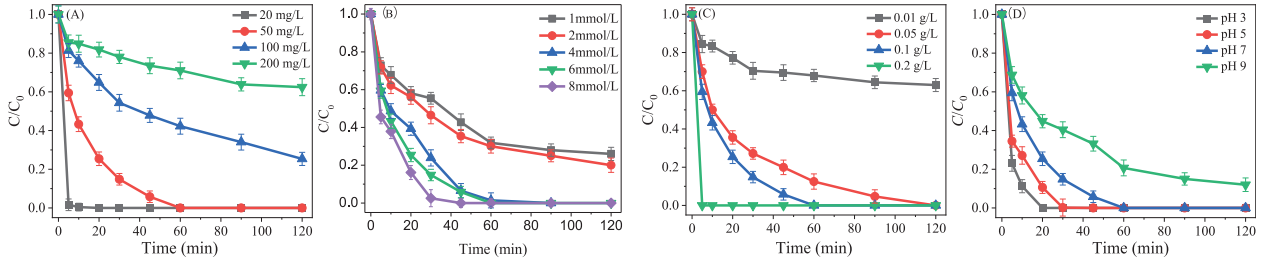

Fig. 2. Effect of the key experimental parameters on SDZ removal in CMK/PDS system. (A) Effect of SDZ concentration: $[PDS]_0 = 6.0$ mmol/L, $[CMK]_0 = 0.1$ g/L, initial pH 7, $[SDZ]_0 = 20$–200 mg/L, and $T = 25 \pm 2$ °C. (B) Effect of PDS concentration: $[PDS]_0 = 1.0$–8.0 mmol/L, $[CMK]_0 = 0.1$ g/L, initial pH 7, $[SDZ]_0 = 50$ mg/L, and $T = 25 \pm 2$ °C. (C) Effect of CMK dosage: $[PDS]_0 = 6.0$ mmol/L, $[CMK]_0 = 0.01$–0.1 g/L, initial pH 7, $[SDZ]_0 = 50$ mg/L, and $T = 25 \pm 2$ °C. (D) Effect of initial pH: $[PDS]_0 = 6.0$ mmol/L, $[CMK]_0 = 0.1$ g/L, initial pH 3–7, $[SDZ]_0 = 50$ mg/L, and $T = 25 \pm 2$ °C.

7.0. Three species of SDZ possibly exist in solution according to its dissociation constants ($pK_{a1} = 1.5$ and $pK_{a2} = 6.5$): SDZ^+, SDZ^0 and SDZ^-. When the pH increased from 3.0 to 9.0, the major species of SDZ changed from neutral to negative. In addition, the change in pH is known to affect the surface charge of CMK [34], thereby affecting the catalytic activity of the heterogeneous system. Under alkaline conditions, sulfate radicals undergo three reactions (Eqs. 1–3) [35]. The self-quenching reaction rate between sulfate radicals (Eq. 3) was significantly higher than that of the other two reactions (Eqs. 1 and 2). Consequently, under alkaline conditions, the total active substances in the system were lower, resulting in a slower degradation rate of the target pollutants in the CMK/PDS system [36].

$$SO_4^{\bullet-} + OH^- \rightarrow SO_4^{2-} + {}^{\bullet}OH \quad (1)$$

$$SO_4^{\bullet-} + SO_4^{\bullet-} \rightarrow S_2O_8^{2-} \quad (2)$$

$$SO_4^{\bullet-} + S_2O_8^{2-} \rightarrow SO_4^{2-} + S_2O_8^{\bullet-} \quad (3)$$

Based on the above results, the RSM using the Box-Behnken model was selected and applied to investigate the optimum value of crucial variables (SDZ concentration, CMK dosage, and PDS concentration) and the interactions among these parameters (Table S1 in Supporting information). Table S2 (Supporting information) shows that the model had high reliability and predictability. It was also found that the order of significance among single factors was as follows: initial SDZ concentration, CMK dosage, and PDS dosage. Among the three variables, the interaction between the initial SDZ concentration and CMK dosage was the most significant (Fig. S4 in Supporting information). The Design-Expert 8.0.6 software was utilized to optimize the parameters of the three factors, with the optimized parameters as follows: Initial SDZ concentration of 44.0 mg/L, the CMK dosage of 0.07 g/L, and PDS dosage of 5.44 mmol/L.

Previous reports found inorganic ions and some natural organic matters would act as radical scavengers in a radical-based oxidation process, thus inhibiting CMK/PDS system performance [37]. Therefore, influence of three common inorganic ions (Cl^-, $H_2PO_4^-$, HCO_3^-) and humic acid (HA) on SDZ degradation were investigated, as shown in Fig. 3. Both Cl^- (5-15 mmol) and $H_2PO_4^-$ (5-15 mmol) exerted no remarkable effect on degradation of SDZ. While, HCO_3^- (5-10 mmol) obviously decreased the degradation efficiency of SDZ (15.0% ± 3.6% ~ 26.0% ± 3.5%) in CMK/PDS system with varied degree, indicating the inhibition to some extent. As HA concentration increased to 40 mg/L, SDZ removal efficiency decreased to 75.0% ± 4.3%, suggesting the slight obstruction of SDZ degradation. Although some of the slight inhibition under relative high concentration was observed, the over-all above 70% of degradation efficiency could be maintained within 60 min. Therefore, we considered the constructed CMK/PDS activation system possessed the relatively high anti-interference ability.

As shown by the Scanning electron microscope (SEM) images in Figs. S5A and B (Supporting information), the microscopic morphology of CMK exhibited a uniform structure. This confirmed that CMK could effectively activate PDS to degrade SDZ after repeated use. Two main components of C and O were revealed in CMK by energy dispersive spectrometer (EDS) spectral analysis, and the O element on the surface of CMK increased after the catalytic reaction slightly (Figs. S5C-F in Supporting information) after the reaction, thus revealing the oxidized surface in an oxygen-rich environment to facilitate PDS activation.

Based on Specific surface area (SSA) analysis and nitrogen adsorption–desorption analysis, the pore sizes of CMK were mainly distributed around 30–50 nm (Figs. S6A and B in Supporting information), which was conducive to providing more active centers for surface catalytic reactions. After the reaction, the SSA decreased from 1188.94 m^2/g to 540.72 m^2/g, which had an important influence on the subsequent adsorption and electron transfer. The reduced BET surface area and pore volume also contributed to the attenuation of the treatment efficiency in subsequent cycles. The Raman spectrum analysis presented two characteristic peaks of CMK, where peak D near 1350 cm^{-1} reflected the degree of disorder, and peak G near 1580 cm^{-1} indicated the level of graphitization (Fig. S6C in Supporting information). Compared with SWCNTs ($I_D/I_G = 0.46$) and MWCNTs ($I_D/I_G = 0.65$), CMK ($I_D/I_G = 1.03$) exhibited a higher degree of disorder. After the reaction, the I_D/I_G ra-

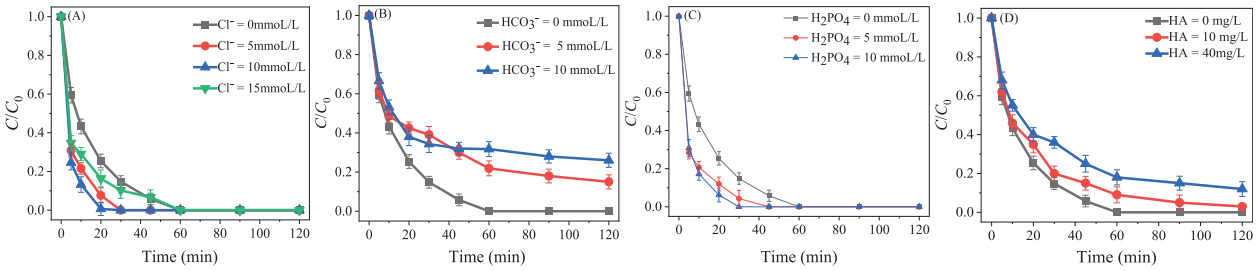

Fig. 3. Effect of water matrices on SDZ removal by CMK/PDS system: (A) Effect of Cl^-, (B) effect of HCO_3^-, (C) effect of $H_2PO_4^-$, (D) effect of humic acid.

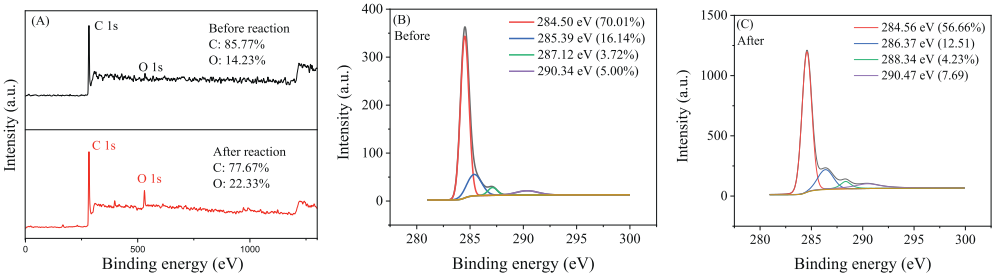

Fig. 4. (A) The XPS full scan image of CMK before reaction and after reaction. (B) The C 1s fine image of CMK before reaction. (C) The C 1s fine image of CMK after reaction.

tio reduced to 0.96 from the original value of 1.03, suggesting a decrease in the degree of defects. The decrease in the degree of defects after the catalytic reaction corresponded well with the decreased catalytic efficiency of CMK in the cycling tests, which demonstrated that the defective sites of CMK were reactive sites for catalyzing PDS.

The X-ray photoelectron spectroscopy (XPS) results revealed that the oxygen content (530.47 eV) increased from 14.23% to 22.33% after the catalytic reaction (Fig. 4A) hence, the oxidized CMK surface was consistent with the EDS energy spectrum analysis. The C 1s peak of the original CMK could be divided into four species with binding energies of 284.50, 285.39, 287.12 and 290.34 eV (Fig. 4B), assigned to C–C, C–OH, C=O and π-π, respectively. The C 1s peak of CMK after the reaction was also fitted into four sections with binding energies of 284.56, 286.37, 288.34, and 290.47 eV (Fig. 4C), corresponding to C–C, C=O, O=C–OH and π-π, respectively. The decrease in C–OH and the increase in C=O and O=C–OH after the reaction indicated that the hydroxyl groups were transformed into carbonyl and carboxyl groups. Combining the above results, the defect structure at the edge of CMK and the oxygen-containing functional groups (especially hydroxyl groups) on the surface of CMK were regarded as potential active sites. Owing to the high SSA and ordered mesoporous structure, a larger adsorption capacity and an increased number of exposed active sites of CMK could be expected, which were considered as the key factors facilitating electron transfer and benefiting oxidation activation.

Radical quenching experiments were carried out using methanol with a $k_{\bullet OH}$ of 9.7×10^8 L mol^{-1} s^{-1} and a $k_{SO_4^{\bullet-}}$ of 3.2×10^6 L mol^{-1} s^{-1}, and ethanol with a $k_{\bullet OH}$ of $(1.6–7.8) \times 10^7$ L mol^{-1} s^{-1} and a $k_{SO_4^{\bullet-}}$ of $(1.2–2.8) \times 10^7$ L mol^{-1} s^{-1}, respectively, to distinguish the contribution of $SO_4^{\bullet-}$ and $^{\bullet}OH$ in the CMK/PDS system [38]. As shown in Fig. 5A, only 89.0% ± 3.1% of SDZ was removed by the CMK/PDS system within 120 min in the presence of methanol at 1000 times the PDS, while this was just 80.3% ± 3.3% for ethanol. Through a comparison of the SDZ degradation efficiencies (Fig. 1), it was suggested that both $SO_4^{\bullet-}$ and $^{\bullet}OH$ were generated and participated in the reaction of the CMK/PDS system, while $^{\bullet}OH$ was slightly dominant over $SO_4^{\bullet-}$. As shown in Fig. 5B, a strong signal of DMPO-$^{\bullet}OH$ adducts was detected at 30 min, and a weak signal of DMPO-$SO_4^{\bullet-}$ adducts was clearly observed, which

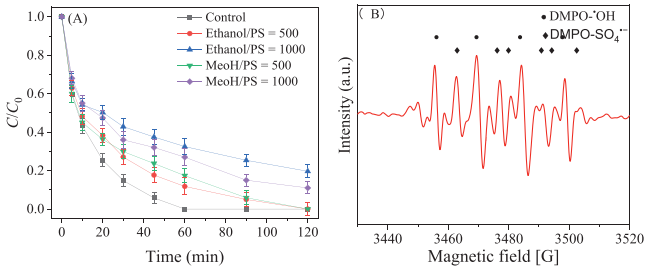

Fig. 5. (A) Effect of scavengers on SDZ degradation by CMK/PDS system. (B) EPR spectra of CMK/PDS system with the existence of DMPO.

could be derived from the fast transformation of DMPO-$SO_4^{\bullet-}$ adducts to DMPO-$^{\bullet}OH$ adducts. These findings support the results of the radical quenching experiment, whereby $^{\bullet}OH$ was slightly more dominant.

Therefore, it is inferred that the free radicals of $SO_4^{\bullet-}$ and $^{\bullet}OH$ were vital to the oxidation system. Combining the Raman spectrum and XPS results (Fig. 4 and Fig. S6), it was inferred that sulfate radicals could be generated by using C–OH and the π electrons flowing at the edge of defects on the surface of CMK to activate PDS and break the O–O bond in persulfate. This was verified by Wang *et al.* [36]. Meanwhile, the free radical quenching results revealed the participation of hydroxyl radicals, which may have been generated by the reaction with the water molecules of partial sulfate radicals [38]. These two types of free radicals functioned together and resulted in the efficient degradation of SDZ, although $^{\bullet}OH$ was slightly more dominant than $SO_4^{\bullet-}$ in the CMK/PDS system. This was consistent with the results of a previous study conducted by Tang *et al.* [31], where CMK was applied to enhance the activation of persulfate during the degradation of 2,4-dichlorophenol. In addition, some studies have found that different from the system with a transition metal as the persulfate activation catalyst [12], nanocarbon-based materials could be applied as electron bridges to facilitate and oxidize SDZ through the direct electron transfer process by activating PDS to form the reaction intermediates [39]. Although the catalytic activity and mechanism were different [40], CMK was reported to possess a higher SSA and larger number of active sites, which may be involved in mediating the electron

transfer of PDS and SDZ. The highly efficient degradation of SDZ was possibly caused by the joint function of $SO^{4\bullet-}$ and $^{\bullet}OH$ oxidation, as well as the promotion of PDS direct oxidation by providing electron channels.

To investigate the degradation pathway of SDZ, the optimized molecular structure of SDZ was obtained using the DFT method (Fig. S7 in Supporting information). The oxidation of SDZ involves a free radical reaction and the electrophilic reaction of SDZ as an electron donor; thus, f^0 was selected to investigate the reaction activity of each atom of the SDZ molecule. As shown in Table S3 (Supporting information), the Fukui function values of the six positions (14S, 1C, 16O, 11 N, 19C and 5C) were relatively large, verifying that these bonds were more likely to be attacked by free radicals and become broken. Based on the DFT model, the SDZ intermediates of radical-induced degradation were investigated using UPLC–MS/MS (Fig. S8 in Supporting information). The intermediate and final metabolites with *m/z* values of 187 (**A**), 114 (**B**), 96 (**C**), 85 (**D**), and 117 (**E** and **F**) were determined. The formation of SO_2 has been frequently reported during the degradation of sulfonamides [41]. In this study, the mass difference between SDZ and product **A** (intermediate $m/z = 187$) was 64, which is exactly equal to the SO_2 loss. Thus, compound **A** was assigned to the product of SO_2 extrusion, which is consistent with the DFT results that the f^0 values of 14S, 15O, and 16O were relatively large; hence, they were easily removed via oxidization. In addition, 2-aminopyrimidine (**C**) is usually regarded as one of the products of S–N bond cleavage during sulfonamide degradation [42]. The f^0 value of 14S was the highest and possessed a high reaction activity, such that the 14S–17 N bond was easily broken. Combined with the mass/nucleus ratio of the intermediate products detected, it could be concluded that product **A** with an *m/z* value of 96 could be **C** due to the attack of the 14S-17 N bond, while **C** was further oxidized to form 2-amino-5-hydroxypyrimidine (**B**) with an *m/z* value of 114. Product **D** with an *m/z* value of 85 and product **B** with an *m/z* value of 114 were formed by 19N–20 N and 19N–27 N cleavage because the f^0 value of 19C was large, which suggested that the cleavage of the C–N bond linking pyrimidine and the benzene ring was also one of the pathways for SDZ degradation [37]. The isomers fumaric acid (**E**) and maleic acid (**F**) with an *m/z* value of 117 were speculated to be formed by the opening of the benzene ring, which was also verified previously by Feng *et al.* (2016) [43].

Based on the above experiments, three potential degradation pathways were proposed for the CMK/PDS system (Fig. S9 in Supporting information). In pathway I, owing to the high f^0 of the 14S (0.539832), 15O (0.148185), and 16O (0.208212) atoms, SDZ could be oxidized to generate product **A** ($m/z = 187$) *via* SO_2 extrusion followed by the rearrangement of atoms. Subsequently, the 6C–19C bond of product **A** continued to be attacked by radicals, resulting in the generation of **C** and aniline. In pathway II, in view of the high $f^0(r)$ value of 19C and the low $f^0(r)$ values of 27 N and 20 N, the cleavage of 19C–27N and 19C–20N bonds could result in the production of intermediates with *m/z* values of 187 (**G**) and 85 (**D**), respectively. Product **G** could be oxidized to aniline, which could be further converted to phenol by a substitution reaction [44]. Then, two products, **F** and **G**, were generated after the ring cleavage of phenol, which was finally oxidized to carbon dioxide and water [43]. In pathway III, considering that the $f^0(r)$ value of 14S was the highest, 14S–17N was easily broken to generate **C** with an *m/z* value of 96 and *p*-aminobenzenesulfonic acid with an *m/z* value of 173. Then, 2-aminopyrimidine was further mineralized to carbon dioxide and nitrate with **B** as the intermediate. *p*-Aminobenzenesulfonic acid was further decomposed with aniline and small molecules of formic acid as the end metabolites. This degradation pathway through S–N bond cleavage is commonly observed during the process of $SO_4^{\bullet-}$ attacking sulfonamides [45].

In this study, highly efficient antibiotic degradation activity was obtained using CMK as the activation material for PDS oxidation (Fig. S1). The superior oxidation ability of the CMK/PDS system was not only reflected in the high degradation of sulfonamides, but also in the degradation of other types of antibiotics with different structures (Fig. S3). Some studies have confirmed that OMC only possesses a two-dimensional nanostructure owing to its rod-like structure [46]. Therefore, compared with traditional carbon nanomaterials, the environmental and biological risks of OMC are greatly reduced [47]. Compared with metal catalytic materials, OMC possesses superior catalytic performance and application potential, reflected in its high efficiency, low toxicity, and biological risk [30]. The catalytic mechanism *via* characterization of CMK (Raman, XPS, BET, and EDS analyses) and analysis of the free radical quenching properties (Fig. 5) revealed that the larger defect sites on the edge of CMK and the oxygen-containing functional groups of CMK promoted electron transfer, while both free radical and non-free radical oxidation processes facilitated the activation of PDS, which finally contributed to the high catalytic efficiency of the system. Three SDZ degradation pathways in the CMK/PDS system were inferred by DFT model calculations and UPLC–MS/MS analysis (Figs. S7 and S8), which were the reaction of 14S–17N cleavage, the removal reaction of the SO_2 molecule by the SDZ molecule, and the reaction of 19C–20N and 19C–28N cleavage of the SDZ molecule. These proposed pathways are consistent with the previously reported oxidative decomposition pathways of SDZ [44], showing a common advanced oxidative degradation law. Although some previous studies have confirmed that OMC can be applied for the catalytic oxidative decomposition of chlorophenols [48], our study verified for the first time that CMK could potentially be applied as a highly efficient, environmentally friendly, and nontoxic catalyst of PDS for the degradation of multiple structures and types of antibiotics.

This study revealed that CMK could be applied as an excellent catalytic material to promote PDS advanced oxidation for the decomposition of sulfonamides and other types of antibiotics with different structures. This study clarified the optimal catalytic parameters. A potential catalytic mechanism was proposed, whereby the defect structure and surface oxidation functional groups of CMK act as activators for generating sulfate radicals and hydroxyl radicals, and CMK acts as a direct electron transfer bridge to oxidize SDZ. Potential SDZ degradation pathways were proposed *via* the direct removal of SO_2 molecules, the 14S–17N fracture, and the 19C–20N and 19C–28N cleavage of the SDZ molecule. Hence, CMK could provide an environmentally friendly and superior catalyst to enhance the oxidation ability of PDS for treating antibiotic-containing wastewater.

Declaration of competing interest

We declare that we have no financial and personal relationships with other people or organizations that can inappropriately influence our work.

Acknowledgments

This study was supported by the NSFC-JSPS joint research program (No. 51961145202) and the Natural Science Foundation of Heilongjiang Province, China (No. C2018035).

Supplementary materials

Supplementary material associated with this article can be found, in the online version, at doi:10.1016/j.cclet.2021.10.086.

References

[1] S. Lu, C. Lin, K. Lei, et al., Water Res. 184 (2020) 116–187.
[2] P. Chaturvedi, P. Shukla, B.S. Giri, et al., Environ. Res. 194 (2021) 110664.
[3] Z. Li, R. Cheng, F. Chen, et al., J. Hazard. Mater. 405 (2021) 124366.
[4] A. Zamora-Galvez, A. Ait-Lahcen, L.A. Mercante, et al., Anal. Chem. 88 (2016) 3578–3584.
[5] S.M. Zainab, M. Junaid, N. Xu, et al., Water Res. 187 (2020) 116–455.
[6] Y. Yang, W. Song, H. Lin, et al., Environ. Int. 116 (2018) 60–73.
[7] C.I. Kosma, M.G. Kapsi, P.G. Konstas, et al., Environ. Res. 191 (2020) 110–152.
[8] J. Cui, L. Fu, B. Tang, et al., Sci. Total Environ. 709 (2020) 136–192.
[9] K. Qin, L. Wei, J. Li, et al., Chin. Chem. Lett. 31 (2020) 2603–2613.
[10] J. Wang, L. Chu, L. Wojnarovits, et al., Sci. Total Environ. 744 (2020) 140–997.
[11] S. Tian, C. Zhang, D. Huang, et al., Chem. Eng. J. 389 (2020) 123–423.
[12] W. Oh, Z. Dong, T. Lim, Appl. Catal. B: Environ. 194 (2016) 169–201.
[13] J. Lee, U. von Gunten, J. Kim, Environ. Sci. Technol. 54 (2020) 3064–3081.
[14] S. Waclawek, H.V. Lutze, K. Grubel, et al., Chem. Eng. J. 330 (2017) 44–62.
[15] R. Yin, B. Jing, S. He, et al., Water Res. 190 (2021) 116720.
[16] X. Yan, D. Yue, C. Guo, et al., Chin. Chem. Lett. 31 (2020) 1535–1539.
[17] R. Yin, Y. Chen, J. Hu, et al., Appl. Catal. B: Environ. 283 (2021) 119663.
[18] U. Ushani, X. Lu, J. Wang, et al., Chem. Eng. J. 402 (2020) 126–232.
[19] X. Duan, H. Sun, S. Wang, Acc. Chem. Res. 51 (2018) 678–687.
[20] Y. Qin, G. Li, Y. Gao, et al., Water Res. 137 (2018) 130–143.
[21] Z. Li, Y. Sun, Y. Yang, et al., Environ. Res. 183 (2020) 109–156.
[22] S. Zhu, X. Huang, F. Ma, et al., Environ. Sci. Technol. 52 (2018) 8649–8658.
[23] Y. Liu, Q. Dai, X. Jin, et al., Environ. Sci. Technol. 52 (2018) 12740–12747.
[24] D.S. Su, S. Perathoner, G. Centi, Chem. Rev. 113 (2013) 5782–5816.
[25] J. Peng, Y. He, C. Zhou, et al., Chin. Chem. Lett. 32 (2021) 1626–1636.
[26] D. Guo, S. You, F. Li, et al., Chin. Chem. Lett. 33 (2022) 1–10.
[27] H. Qiu, P. Guo, L. Yuan, et al., Chin. Chem. Lett. 31 (2020) 2614–2618.
[28] H. Lee, H. Kim, S. Weon, et al., Environ. Sci. Technol. 50 (2016) 10134–10142.
[29] W. Ren, L. Xiong, G. Nie, et al., Environ. Sci. Technol. 54 (2020) 1267–1275.
[30] M.R. Benzigar, S.N. Talapaneni, S. Joseph, et al., Chem. Soc. Rev. 47 (2018) 2680–2721.
[31] L. Tang, Y. Liu, J. Wang, et al., Appl. Catal. B: Environ. 231 (2018) 1–10.
[32] H. Sun, C. Kwan, A. Suvorova, et al., Appl. Catal. B: Environ. 154 (2014) 134–141.
[33] D. Huang, Q. Zhang, C. Zhang, et al., Chem. Eng. J. 391 (2020) 123–532.
[34] Q. Sui, J. Huang, Y. Liu, et al., J. Environ. Sci. China 23 (2011) 177–182.
[35] C. Liang, Z. Wang, C.J. Bruell, Chemosphere 66 (2007) 106–113.
[36] H. Wang, W. Guo, B. Liu, et al., Water Res. 160 (2019) 405–414.
[37] C. Zhu, F. Zhu, D.D. Dionysiou, et al., Water Res. 139 (2018) 66–73.
[38] W. Yang, X. Li, Z. Jiang, et al., Appl. Surf. Sci. 525 (2020) 146–482.
[39] J. Yu, H. Feng, L. Tang, et al., Prog. Mater. Sci. 111 (2020) 100–654.
[40] E. Yun, H. Yoo, H. Bae, et al., Environ. Sci. Technol. 51 (2017) 10090–10099.
[41] A.L. Boreen, W.A. Arnold, K. McNeill, Environ. Sci. Technol. 39 (2005) 3630–3638.
[42] Y. Liu, J. Wang, J. Hazard. Mater. 250 (2013) 99–105.
[43] Y. Feng, D. Wu, Y. Deng, et al., Environ. Sci. Technol. 50 (2016) 3119–3127.
[44] Y. Zhang, S. Hu, H. Zhang, et al., Sci. Total Environ. 607 (2017) 1348–1356.
[45] Y. Yang, X. Lu, J. Jiang, et al., Water Res. 118 (2017) 196–207.
[46] B. Szczesniak, J. Choma, M. Jaroniec, Chem. Commun. 56 (2020) 7836–7848.
[47] S.R. Pinto, E. Helal-Neto, F. Paumgartten, et al., Artif. Cell. Nanomed. B 462 (2018) 527–538.
[48] P. Guo, H. Qiu, C. Yang, et al., J. Hazard. Mater. 402 (2021) 123846.